Structural phase transition and dynamical properties of $PbTiO_3$ simulated by molecular dynamics



2005 J. Phys.: Condens. Matter 17 5771

(http://iopscience.iop.org/0953-8984/17/37/013)

INSTITUTE OF PHYSICS PUBLISHING JOURNAL OF PHYSICS: CONDENSED MATTER

J. Phys.: Condens. Matter **17** (2005) 5771–5783 doi:10.1088/0953-8984/17/37/013

# Structural phase transition and dynamical properties of $PbTiO_3$ simulated by molecular dynamics

**S C Costa[1], P S Pizani[1], J P Rino[1] and D S Borges[2]**

[1] Universidade Federal de São Carlos, Departamento de Física, Caixa Postal 676-13565-905 São Carlos, SP, Brazil
[2] Departamento de Ensino e Pesquisa do Ministério do Exército, Colégio Militar de Manaus—CMM, Rua José Clemente, 0157, Centro, 69010-070 Manaus, Amazonas, Brazil

E-mail: sancosta@df.ufscar.br

Received 20 June 2005
Published 2 September 2005
Online at stacks.iop.org/JPhysCM/17/5771

**Abstract**

The temperature- and pressure-induced structural phase transition in $PbTiO_3$ is studied with the isoenthalpic–isobaric molecular-dynamics method, using an effective two-body interaction potential. The tetragonal to cubic transformation is successfully reproduced with both temperature and pressure. The behaviour of lattice parameters, vibrational density of states, and phonon anharmonicity with temperature and pressure are in very good agreement with experimental data. Two- and three-body correlations were analysed through pair distribution functions, coordination numbers and bond-angle distributions.

## 1. Introduction

The $ABO_3$-type perovskites (A = Ba, Ca, Pb, Sr and B = Ti, Zr) form one of the most important class of ferroelectric materials with nonlinear electro-optical properties, and they can be employed in several applications in electronic technology [1]. The majority of these materials shows a paraelectric to ferroelectric temperature- and/or hydrostatic pressure-induced phase transition. In particular, $PbTiO_3$ (PT) shows the cubic-paraelectric to tetragonal-ferroelectric phase transition at about 770 K at atmospheric pressure and at about 12 GPa at room temperature; these results were obtained experimentally [2–4]. In the ferroelectric phase, it has a large tetragonal distortion (thus the parameters associated with the polar phase, such as spontaneous polarization and ionic shifts, are considerably large), high Curie temperature and a wide temperature range in which the tetragonal phase is stable [5]. It is also known that the temperature of the phase transition decreases with increasing the hydrostatic pressure [6, 7]. Despite its scientific and technological importance, few theoretical and computational simulations can be found in the literature. Only papers using mainly density functional theory for lattice dynamics and electronic band structure studies can be found [8].

In this paper, we point out that isoenthalpic–isobaric molecular dynamics (MD) simulations give a stable tetragonal phase for the low pressure and temperature range and can describe the temperature- and pressure-induced structural tetragonal to cubic phase transition in lead titanate. Furthermore, dynamical properties such as the vibrational density of states, temperature and pressure phonon anharmonicity, and dynamical Debye–Waller factor are simulated or predicted.

## 2. Interaction potential and molecular dynamics calculation

The literature presents a large variety of empirical interaction potentials that describe materials from elemental semiconductors to more complex systems [9, 10]. The potential chosen by us was one proposed by Vashishta and Rahman, which has been used successfully for many different systems for about 30 years [11–17]. The total interaction potential is:

$$\Phi = \sum_{i \prec j}^{N} \left[ \frac{H_{\alpha\beta}}{r_{ij}^{\eta_{\alpha\beta}}} + \frac{Z_{\alpha\beta} e^{-r/\lambda}}{r_{ij}} - \frac{D_{\alpha\beta} e^{-r/\xi}}{2r_{ij}^4} - \frac{W_{\alpha\beta}}{r_{ij}^6} \right], \tag{1}$$

where $N$ is the number of atoms, $r_{ij} = |\vec{r}_{ij}|$, $\vec{r}_{ij} = \vec{r}_i - \vec{r}_j$, and $\vec{r}_i$ is the position of the $i$th atom. $\alpha$ and $\beta$ denote the atomic species. The first term represents steric repulsion (with parameters $H_{\alpha\beta}$ and $\eta_{\alpha\beta}$), the second is the Coulomb interaction, the third is the charge-induced dipole interaction due to the large electronic polarizability of ions, and the last is the van der Waals (dipole–dipole) type interaction. The screenings in the Coulomb and charge–dipole interactions are introduced in order to avoid the long-range calculations of these interactions. The range of the screening was fixed respectively at $\lambda = 0.50$ nm and $\xi = 0.35$ nm, and the two-body potential is truncated at $r_c = 0.9$ nm. The interaction potential for $r < r_c$ is shifted in the usual way [22], in order to ensure that the potential and its first derivative have continuous values at the cut-off length. From other simulations using this type of potential we took the exponents $\eta_{\mathrm{PbPb}}$, $\eta_{\mathrm{PbTi}}$, $\eta_{\mathrm{PbO}}$, $\eta_{\mathrm{TiTi}}$, $\eta_{\mathrm{TiO}}$, and $\eta_{\mathrm{OO}}$ to be 11, 9, 7, 11, 9, and 7 respectively [12, 17]. The effective charges $Z_\alpha$ were obtained from first principles (density functional theory) electronic structure calculations by E Orhan (private communication). A detailed discussion of the application of this model for $SrTiO_3$ can be found in [18, 19]. The remaining constants were optimized from the elastic constant, bulk modulus, and melting/decomposition temperature and the lattice stability in room conditions. It is worth mentioning that there are several type of potentials that are well able to describe a given material. In the particular case of the $ABO_3$ perovskites, Akhtar *et al* [20] (for $SrTiO_3$) and Lewis *et al* [21] (for $BaTiO_3$) obtained good results using full ionic charges.

The simulations were performed in the isoenthalpic–isobaric ensemble due to Parrinello and Rahman, which allows the simulation box to change in size and shape [23], as well the as micro-canonical ensemble. The system consists of 1715 particles (343 Pb, 343 Ti, and 1029 O) initially arranged in a tetragonal perovskite structure at the actual density of PT, with zero external pressure. The system was generated at 100 K and studied in two ways. In one way the pressure was kept at zero GPa and the system was stepwise heated to a temperature of 2000 K. The temperature was allowed to fluctuate 1% by scaling the velocity of particles every time step. In the other study, at a temperature of 300 K the external pressure was raised at a rate of 0.5 GPa per 50 000 time steps (one time step is 2.29 fs) up to 12 GPa. In both cases averages were taken over an additional 20 000 time steps to obtain two- and three-body correlation functions such as the pair distribution function, coordination number and bond-angle distributions.

The phase space trajectory obtained from the MD simulation allows us to determine the pair distribution function (PDF), which furnishes the bond distance between pairs of atoms.

From the PDF we can also obtained the temperature dependence of the atomic oscillation amplitude $\Delta x$ for the atoms and consequently the dynamical Debye–Waller factor [24],

$$D(T) = \exp[-2M(T)] = \exp\left[\frac{-4\pi^2(\Delta x)^2}{3d^2}\right], \tag{2}$$

where $d$ is the lattice spacing for the planes giving rise to the reflection under consideration.

The vibrational density of states $G(\omega)$ can be obtained from the Fourier transform of the velocity–velocity correlation function $Z_\alpha(t)$ [22]:

$$G_\alpha(\omega) = \frac{6N_\alpha}{\pi}\int_0^\infty Z_\alpha(t)\cos(\omega t)\,\mathrm{d}t, \tag{3}$$

with $Z_\alpha(t)$ defined as

$$Z_\alpha(t) = \frac{\langle v_{i\alpha}(0)\cdot v_{i\alpha}(t)\rangle}{\langle v_{i\alpha}(0)^2\rangle}, \tag{4}$$

where $v_{i\alpha}(t)$ is the velocity of particle $i$ of type $\alpha$ at time $t$, and $\langle\,\rangle$ denotes an ensemble average over all particles of type $\alpha$. From the resulting MD simulations we can obtain the temperature and pressure dependence of the maxima of the vibrational density of states, that is the phonon anharmonicity. A linear approximation gives the pressure frequency coefficient $(\partial\omega/\partial P)_T$ and the temperature frequency coefficient $(\partial\omega/\partial T)_P$, related by

$$\left(\frac{\partial\omega}{\partial T}\right)_P = \left(\frac{\partial\omega}{\partial T}\right)_V - \gamma B\left(\frac{\partial\omega}{\partial P}\right)_T \tag{5}$$

where the first term on the right-hand side denotes the self-energy shift, the second term the purely volume-dependent part, $\gamma$ is the volumetric thermal expansion coefficient and $B$ the bulk modulus.

## 3. Results and discussion

The set of experimental values reported in the literature [25, 26] which were used as a guide for determining the parameters in the interaction potential (equation (1)) is displayed in table 1 along with the results of the MD simulation, obtained at 100 K. This interaction potential provides stable perovskite structures (tetragonal and cubic) for all temperatures and pressures studied. Once the results from the simulations reproduce the experimental values and structure well, the potential parameters (see table 2) are fixed to simulate all other properties.

### *3.1. Structural analysis: temperature effect*

The tetragonal to cubic structural phase transition induced by temperature is shown in figure 1, where the lattice parameters are displayed as a function of $T/T_c$, together with experimental data [3, 27]. The lattice parameters converge to the same value, showing a jump at approximately 1100 K, indicating the phase transition. The high value of the simulated $T_c$ compared with the experimental one can be attributed to the periodic boundary conditions imposed on the system in the simulation method. In the low temperature range the simulation reproduces the lattice contraction well, leading to a negative volumetric thermal expansion, as observed experimentally [3, 25, 28, 29]. A linear approximation in the low simulation temperature range, from 10 to 100 K, furnishes the linear thermal expansion coefficients $\alpha_c \sim -8\times10^{-5}\ \mathrm{K}^{-1}$ and $\alpha_a = \alpha_b \sim 4\times10^{-5}\ \mathrm{K}^{-1}$, giving a small volumetric expansion coefficient $\gamma \sim -0.1\times10^{-5}\ \mathrm{K}^{-1}$, coherent with experimental results that show a zero crossing at 300 K [3]. However, in the high temperature range, still

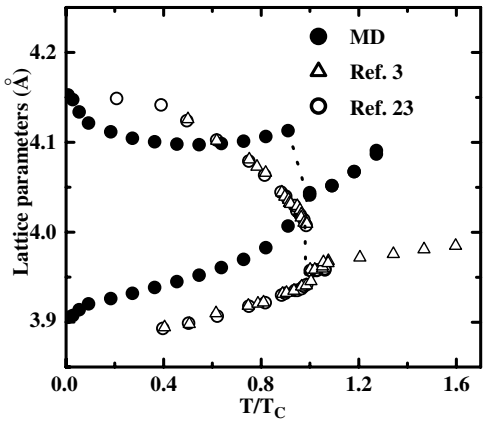


**Figure 1.** The temperature evolution of the lattice parameters, showing the structural tetragonal to cubic phase transition. The solid circles are MD simulations and the open symbols are experimental data [3, 27]. The dotted lines are visual guides.

**Table 1.** Experimental and MD values of the lattice parameter, elastic constants, bulk modulus, and melting/decomposition temperature of $PbTiO_3$.

| | Experiments [25, 26] | Molecular dynamics |
|---|---|---|
| Lattice parameters (Å) | | |
| $a$ | 3.895 | 3.904 |
| $c$ | 4.171 | 4.153 |
| Elastic constants (GPa) | | |
| $C_{11}$ | $237 \pm 3$ | 293.4 |
| $C_{33}$ | $60 \pm 10$ | 96.8 |
| $C_{44}$ | $69 \pm 1$ | 90 |
| $C_{66}$ | $104 \pm 1$ | 95.6 |
| $C_{12}$ | $90 \pm 5$ | 95.0 |
| $C_{13}$ | $70 \pm 10$ | 81.9 |
| Bulk modulus (GPa) | 110.44 | 135 |
| Melting/decomposition temperature (K) | 1300 | $2000 \pm 50$ |

in the tetragonal phase, approaching $T_c$, the simulation gives a lattice expansion, contrary to the experimental behaviour. For the cubic phase, the thermal expansion coefficients show an isotropy in which $\alpha_a$, $\alpha_b$, and $\alpha_c \sim 4 \times 10^{-5}$ K$^{-1}$, in good agreement with experimental data ($\alpha_a = \alpha_b = \alpha_c \sim 6 \times 10^{-5}$ K$^{-1}$) [3].

Additional information of the structural phase transition can be obtained from the temperature variation of the pair distribution function, shown in figure 2, which gives the bond-length distance and the coordination number between two Pb atoms. For temperatures lower than $T_c$, the Pb–Pb bond distance and coordination number display two different values, characteristic of the tetragonal phase. After the transition, there is just one bond distance and coordination number, typical of cubic symmetry. The dotted lines are Gaussian fittings that make clear the two bond distances in the tetragonal phase. For intermediate temperature this analysis is fundamental once the distances are hidden by thermal agitation. From the full width of the two first peaks, the atomic oscillation amplitude $\Delta x$ and its temperature dependence were obtained, as displayed in figure 3. From a linear fit approximation, the temperature coefficient for $(\Delta x)^2$ was obtained: $(\partial(\Delta x)^2/\partial T) = 1.5 \times 10^{-6}$ nm$^2$ K$^{-1}$ for the first peak

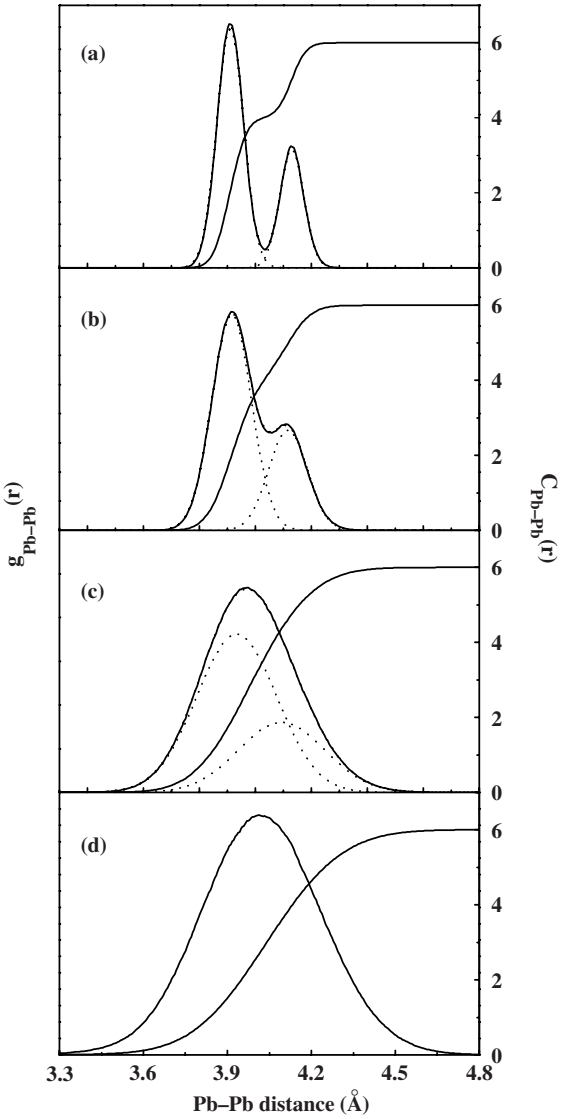


**Figure 2.** The Pb–Pb pair distribution function $g_{Pb-Pb}(r)$ (left) and coordination number $C_{Pb-Pb}(r)$ (right) at zero pressure at (a) 60 K, (b) 100 K, (c) 500 K, and (d) 1100 K. At 500 K the system is still tetragonal but the thermal agitation broadens the PDF peaks.

(vibration along $a$- and $b$-axis) and $(\partial(\Delta x)^2/\partial T) = 1.8 \times 10^{-6}$ nm$^2$ K$^{-1}$ for the second peak ($c$-axis). These results, with equation (5), can be used to predict the temperature dependence of the Debye–Waller factor.

The temperature effect on the structural symmetry was also analysed through three-body correlation. In figure 4 we show the Pb–O–Pb bond-angle distribution for three different temperatures. Due to thermal agitation the peaks are superposed at high temperatures, being better seen by fitting Gaussians (dotted lines in the figure). As the temperature increases, the three peaks characteristic of the tetragonal phase evolute to 90°, which is typical of the cubic perovskite structure.

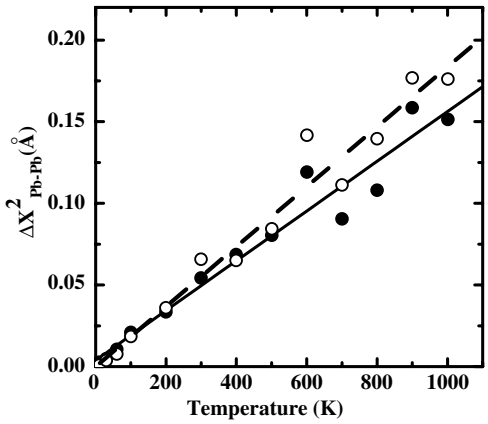


**Figure 3.** The temperature dependence of $(\Delta x)^2$ for the first (full circles) and second (open circles) peaks in $g_{Pb-Pb}(r)$. Linear fits, continuous line for the former and dashed line for the latter, gave the coefficients $(\partial(\Delta x)^2/\partial T)_P$.

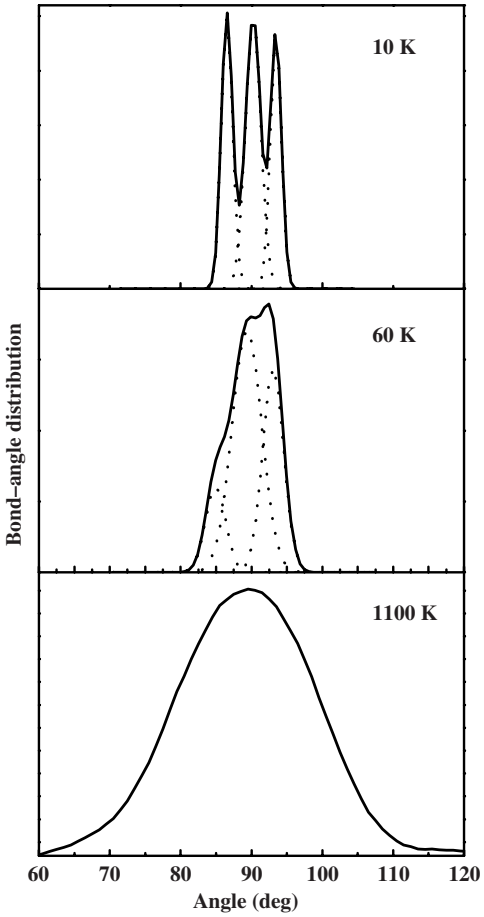


**Figure 4.** Pb–O–Pb bond-angle distributions at zero pressure for three different temperatures. At 10 K the presence of angles distinct from 90° characterizing the tetragonal structure can be seen.

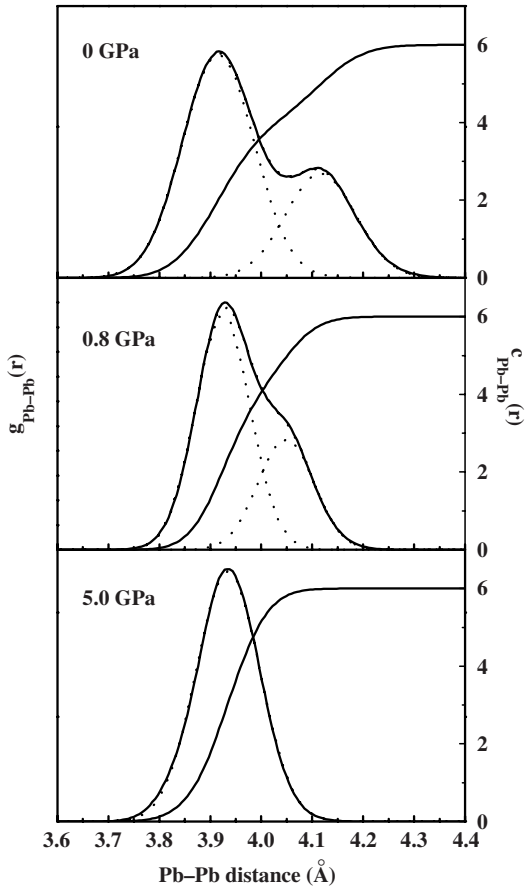


**Figure 5.** The Pb–Pb pair distribution function $g_{Pb-Pb}(r)$ (left) and coordination number $C_{Pb-Pb}(r)$ (right) around Pb atoms at 100 K at (a) 0 GPa, (b) 0.8 GPa, and (c) 5.0 GPa where the transition occurs.

### *3.2. Structural analysis: pressure effect*

Figure 5 shows the evolution of the Pb–Pb PDF and coordination number for three different pressures at 100 K; the tetragonal to cubic phase transition is very well reproduced. To obtain the lattice parameters, we performed Gaussian fittings (dotted lines) since the two peaks are superposed due to the thermal agitation, mainly for temperatures and/or pressures near the transition value. The lattice parameter dependence on the hydrostatic pressure at 100, 200 and 300 K is displayed in figure 6, together with experimental data taken at 462, 538 and 623 K. The lowering of the transition pressure value with increasing temperature is well described, showing a very good agreement. A linear fit in the range up to 2.0 GPa at 100 K furnishes $\mathrm{d}a/\mathrm{d}P = 10\times10^{-3}$ Å $\mathrm{GPa}^{-1}$ and $\mathrm{d}c/\mathrm{d}P = -8\times10^{-2}$ Å $\mathrm{GPa}^{-1}$, in agreement with experimental results at room temperature: $\sim2\times10^{-3}$ Å $\mathrm{GPa}^{-1}$ and $\sim-6\times10^{-2}$ Å $\mathrm{GPa}^{-1}$, respectively [30]. The pressure-induced phase transition is also well described from the bond-angle distribution as we can see in figure 7, which shows the distinct bond angles of the tetragonal phase which evolute to 90° of the cubic phase by applying hydrostatic pressure.

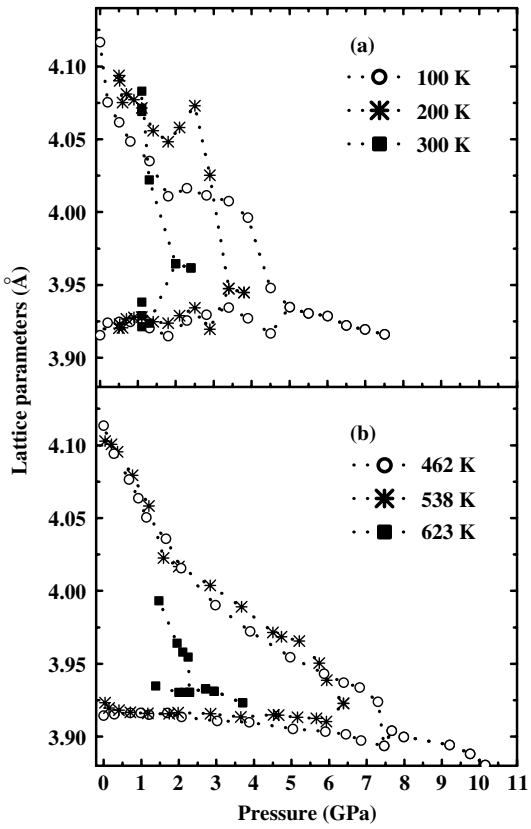


**Figure 6.** Simulated and measured evolution of lattice parameters with pressure at different temperatures. (a) Simulation data and (b) experimental data. The data were arranged to give an idea of the phase diagram.

**Table 2.** Parameters used in the interaction potential of equation (1) for $PbTiO_3$ (energy in ergs and distances in nanometres).

| | Pb–Pb | Pb–Ti | Pb–O | Ti–Ti | Ti–O | O–O |
|---|---|---|---|---|---|---|
| $H_{\alpha\beta}$ | $1.0378 \times 10^{-7}$ | $1.4943 \times 10^{-9}$ | $6.3421 \times 10^{-10}$ | $7.2681 \times 10^{-10}$ | $4.8635 \times 10^{-10}$ | $4.6120 \times 10^{-10}$ |
| $Z_{\alpha\beta}$ | $1.025e^2$ | $2.2995e^2$ | $-1.134e^2$ | $4.7961e^2$ | $-2.3652e^2$ | $1.1664e^2$ |
| $D_{\alpha\beta}$ | $1.764e^2$ | $2.0696e^2$ | $1.2474e^2$ | $0.9592e^2$ | $0.9461e^2$ | $0.6998e^2$ |
| $W_{\alpha\beta}$ | $7.39 \times 10^{-12}$ | $7.39 \times 10^{-12}$ | $7.39 \times 10^{-12}$ | $7.39 \times 10^{-12}$ | $4.39 \times 10^{-12}$ | $7.39 \times 10^{-12}$ |
| $\eta_{\alpha\beta}$ | 11 | 9 | 7 | 11 | 9 | 7 |
| $\lambda = 0.50$ nm | $\xi = 0.35$ nm | $r_{cut} = 0.9$ nm | $e =$ electron charge | | | |

### *3.3. Dynamical analysis*

The vibrational density of states $G(\omega)$ obtained by the MD simulation is displayed in figure 8 with the theoretical dispersion curve (whose projection on the horizontal axis reflects the vibrational density of states) obtained by using the rigid ion model [31] and the Raman spectrum at room temperature [32]. The results obtained from MD fit both theoretical and experimental results very well, reproducing correctly the frequencies of the acoustic and optical bands. The small shifts in the absolute value of the frequencies may be attributed to the effects of the size of the simulation box and to temperature and pressure effects.

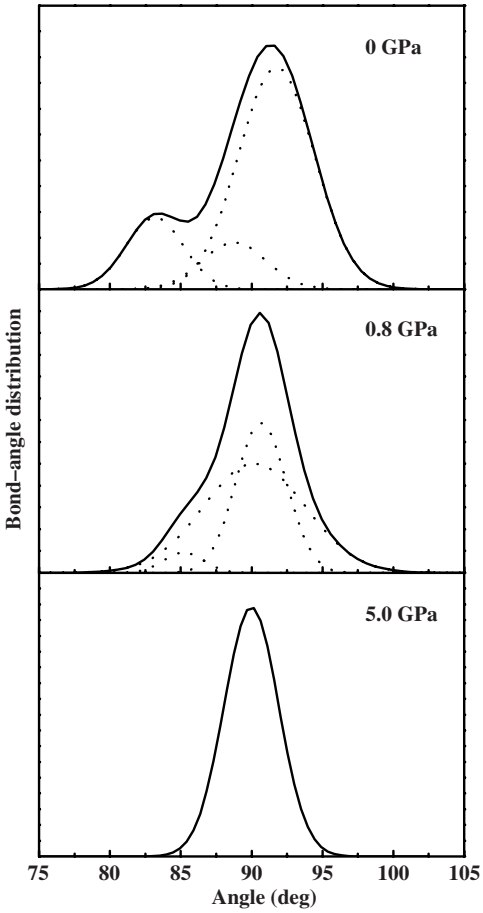


**Figure 7.** Pb–O–Pb bond angles at 100 K. At 0 GPa the presence of angles distinct from 90° characterizing the tetragonal structure can be seen.

The temperature effect on $G(\omega)$, that is, the anharmonic effect, is shown in figure 9, which displays $G(\omega)$ for three different temperatures. The results from the MD simulations can be seen in figure 10, which shows the temperature dependence of the eight principal maxima of $G(\omega)$, along with the experimental data from Raman scattering [33]. Although Raman scattering samples only phonons at the centre of the Brillouin zone, the general behaviour, such as the 'softening' and the broadening of some peaks, normally expected for the majority of materials, is correctly reproduced. The evolution of the 'soft mode' cannot be studied from our MD results since it is masked by the acoustical band. From a linear approximation the temperature frequency coefficients $(\partial\omega/\partial T)_P$ for each maximum of $G(\omega)$ were obtained, and they are displayed in table 3.

Figure 11 shows the evolution of $G(\omega)$ at 300 K, for three different pressures, revealing the 'hardening' of the vibrational modes, normally observed for the majority of materials. Figure 12 shows the pressure dependence of the eight maxima of $G(\omega)$ and the experimental results from Raman scattering [4], showing that the general behaviour is correctly reproduced by the MD simulation. Again we can obtain the pressure frequency coefficients $(\partial\omega/\partial P)_T$ for each maximum of $G(\omega)$ from linear approximation. From the simulated values of the

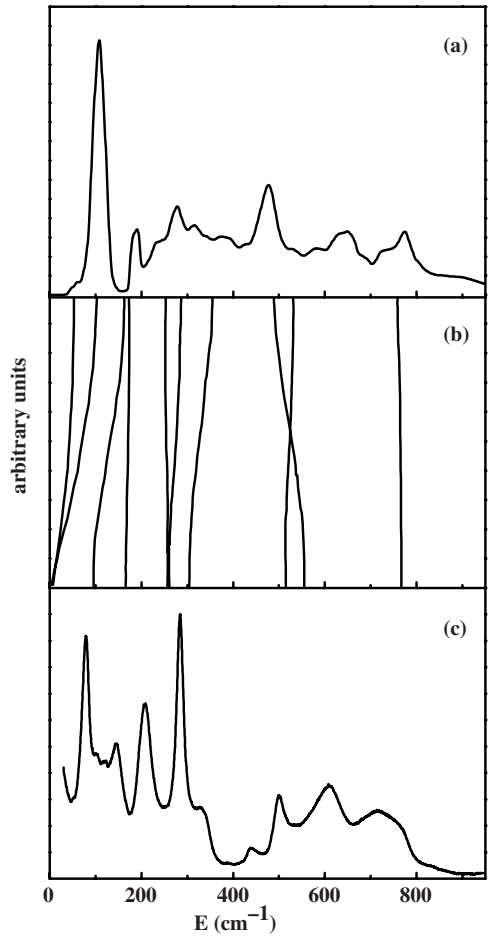


**Figure 8.** (a) Vibrational density of states, $G(\omega)$, from the molecular dynamics simulation at 0 GPa and 300 K. (b) Phonon dispersion curve whose projection on the horizontal axis reflects the vibrational density of states [31]. (c) Raman spectrum [32].

**Table 3.** Calculated temperature frequency coefficients of the eight maxima of the vibrational density of states of $PbTiO_3$.

| | $\omega_1$ | $\omega_2$ | $\omega_3$ | $\omega_4$ | $\omega_5$ | $\omega_6$ | $\omega_7$ | $\omega_8$ |
|---|---|---|---|---|---|---|---|---|
| $\omega$ (cm$^{-1}$) | 110 | 250 | 320 | 380 | 480 | 640 | 775 | 865 |
| $\left(\frac{\partial\omega}{\partial T}\right)_P$ (cm K$^{-1}$) | −0.004 | 0.003 | −0.016 | 0.001 | −0.019 | −0.028 | −0.012 | −0.033 |
| $\left(\frac{\partial\omega}{\partial P}\right)_T$ (cm GPa$^{-1}$) | 1.2 | 0.3 | −0.7 | 0.4 | 2.1 | 6.6 | 3.1 | 10.9 |
| $\left(\frac{\partial\omega}{\partial T}\right)_V$ (cm K$^{-1}$) | −0.08 | 0.02 | −0.04 | −0.29 | −0.17 | −0.52 | −0.24 | −0.84 |

coefficients $(\partial\omega/\partial T)_P$, $(\partial\omega/\partial P)_T$, the experimental thermal expansion [27] $\gamma = -6.75 \times 10^{-4}$ K$^{-1}$, and bulk modulus $B = 110$ GPa, the coefficient $(\partial\omega/\partial T)_V$ was calculated using equation (5). All values of these coefficients are collected in table 3.

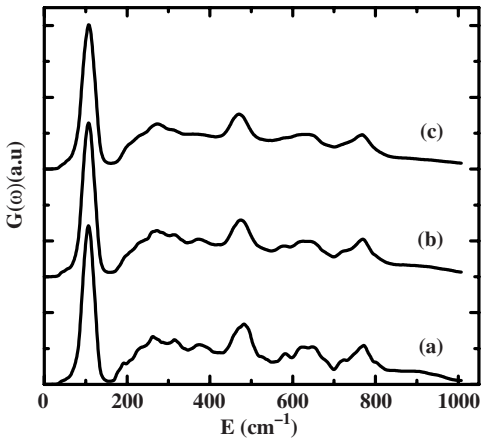


**Figure 9.** Temperature dependence of $G(\omega)$ from MD simulation at (a) 300 K (b) 600 K (c) 900 K.

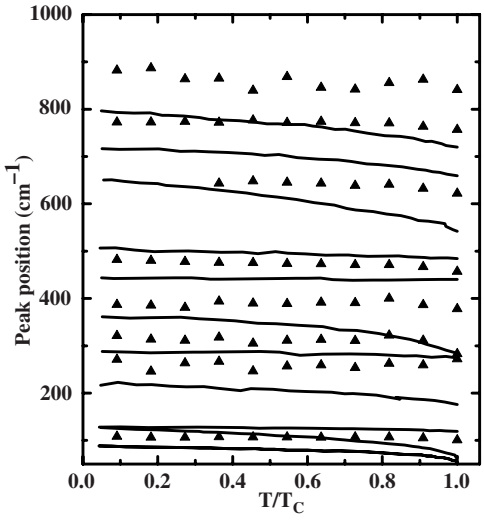


**Figure 10.** Experimental and simulated temperature dependence of the frequency modes. The dotted lines are from experimental data [33] and full symbols are from MD simulations.

## 4. Conclusions

Summarizing, we have performed a Parrinello–Rahman molecular dynamics simulation for the structural and dynamical properties of lead titanate, using an effective potential which takes into account two-body interactions. From the pair distribution function and bond-angle distribution, structural properties such as crystal symmetry and coordination number were obtained, in excellent accord with the experimental data. The two polymorphic phases were correctly described and the corresponding phase transition as a function of hydrostatic pressure and temperature was also simulated, showing that the proposed interatomic potential is able to describe the tetragonal to cubic phase transition of $PbTiO_3$. From the temperature dependence of the full width of the pair distribution function the atomic amplitude oscillation

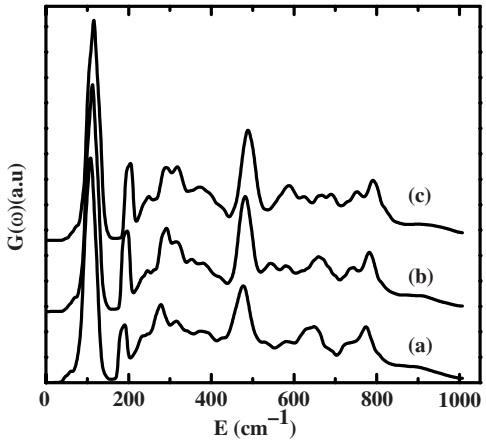


**Figure 11.** Pressure dependence of $G(\omega)$ from MD simulation at (a) 0 GPa (b) 2.3 GPa (c) 5.5 GPa.

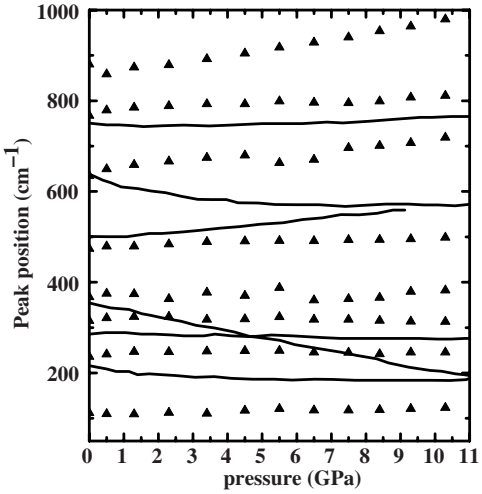


**Figure 12.** Experimental and simulated pressure dependence of the frequency modes. The dotted lines are from experimental data [4] and full symbols are from MD simulations.

was obtained, which permits us to predict the temperature dependence of the Debye–Waller factor, an important parameter that reflects the configurational disorder. From the temperature variation of the simulation box sides the linear thermal expansion coefficients of the tetragonal phase for each of the three crystalline axes were determined, revealing a strong anisotropy along the polar tetragonal *c*-axis. Although the numerical value of the volumetric expansion obtained from the simulation disagrees with the experimental one, the general behaviour such as negative volumetric thermal expansion was correctly reproduced for low temperatures. In addition, the pressure and temperature dependence of the vibrational density of states (phonon anharmonicity) was also correctly described, showing a coherent behaviour if compared with experimental data from Raman scattering. Finally, the pressure and temperature frequency coefficients were determined, including the self-energy term.

## Acknowledgments

This work was supported by the Brazilian research-financing agencies FAPESP, CNPq and CAPES.

## References

[1] Schwarts R N, Wechsler B A and West L 1995 *J. Appl. Phys.* **67** 1352
[2] Shirane G, Pepisnky R and Frazer B C 1956 *Acta Crystallogr.* **9** 131
[3] Xing X, Deng J, Chen J and Guirong L 2003 *Rare Met.* **22** 294
[4] Sanjurjo J A, Lopez-Cruz E and Burns G 1983 *Phys. Rev.* B **28** 7260
[5] Shirane G, Axe J D, Harada J and Remeika J P 1970 *Phys. Rev.* B **2** 155
[6] Zha C S, Kalinichev A G, Bass J D, Suchicital C T A and Payne D A 1992 *J. Appl. Phys.* **72** 3705
[7] Sani A, Hanfland M and Levy D 2002 *J. Solid State Chem.* **167** 446
[8] Ghosez Ph, Cockayne E, Waghmare U V and Rabe K M 1999 *Phys. Rev.* B **60** 836
[9] Stillinger F H and Weber T A 1985 *Phys. Rev.* B **31** 5262
[10] Erkoç S 1997 *Phys. Rep.* **278** 79
[11] Vashishta P and Rahman A 1978 *Phys. Rev. Lett.* **40** 1337
[12] Parrinello M, Rahman A and Vashishta P 1983 *Phys. Rev. Lett.* **50** 1073
[13] Nakano A, Kalia R K and Vashishta P 1994 *J. Non-Cryst. Solids* **171** 157
[14] Shimojo F, Ebbsjo I, Kalia R K, Nakano A, Rino J P and Vashishta P 2000 *Phys. Rev. Lett.* **84** 3338
[15] Rino J P, Chatterjee A, Ebbsjo I, Kalia R K, Nakano A, Shimojo F and Vashishta P 2002 *Phys. Rev.* B **65** 195206
[16] Costa S C, Pizani P S and Rino J P 2002 *Phys. Rev.* B **66** 214111
Costa S C, Pizani P S and Rino J P 2003 *Phys. Rev.* B **68** 073204
[17] Branicio P S, Rino J P, Shimojo F, Li W, Kalia R K, Nakano A and Vashishta P 2003 *J. Appl. Phys.* **94** 3840
[18] Orhan E, Pontes F M, Pinheiro C D, Boschi T M, Leite E R, Pizani P S, Beltrán A, Andrés J, Varela J A and Longo E 2004 *J. Solid State Chem.* **177** 3879
[19] Longo E, Orhan E, Pontes F M, Pinheiro C D, Leite E R, Varela J A, Pizani P S, Boschi T M, Lanciotti F, Beltrán A and Andrés J 2004 *Phys. Rev.* B **69** 125115
[20] Akhtar M J, Akhtar Z-U-N and Jackson R A 1995 *J. Am. Ceram. Soc.* **78** 421
[21] Lewis G V and Catlow C R A 1986 *J. Phys. Chem. Solids* **47** 89
[22] Allen M P and Tildesley D J 1997 *Computer Simulation of Liquids* (Oxford: Clarendon)
[23] Parrinello M and Rahman A 1980 *Phys. Rev. Lett.* **45** 1196
Parrinello M and Rahman A 1981 *J. Appl. Phys.* **52** 7182
[24] Guinier A 1963 *X-Ray Diffraction in Crystals, Imperfect Crystals and Amorphous Bodies* (San Francisco, CA: Freeman)
[25] Glazer A M and Mabud S A 1978 *Acta Crystallogr.* **34** 1065
[26] Kalinichev A G, Bass J D, Sun B N and Payne D A 1997 *J. Mater. Res.* **12** 2623
[27] Shirane G, Hoshino S and Suzuki K 1950 *Phys. Rev.* **80** 1105
[28] Kobayashi J, Uesu Y and Sakemi Y 1983 *Phys. Rev.* B **28** 3866
[29] Nelmes R J and Kuhs W F 1985 *Solid State Commun.* **54** 721
[30] Nelmes R J and Katrusiak A 1986 *J. Phys. C: Solid State Phys.* **19** L725
[31] Freire J D and Katiyar R S 1988 *Phys. Rev.* B **37** 2074
[32] Tavares E C S, Pizani P S and Eiras J A 1998 *Appl. Phys. Lett.* **72** 837
[33] Burns G and Scott an B 1973 *Phys. Rev.* B **73** 3088